Biointerface Research in Applied Chemistry
Open-Access Journal (ISSN: 2069-5837)

Article
Volume 13, Issue 4, 2023, 380
https://doi.org/10.33263/BRIAC134.380

Corrosion Inhibition Investigation of Small Organic Inhibitor on API5LX60 Steel in 3.5% NaCl Solution with CO_2 Saturation

Parijat Burhagohain [1], Gitalee Sharma [2,*], Prankush M. Bujarbaruah [3], Uddipana S. Deka [4], Dipak J. Kalita [5]

[1] Department of Chemistry, Dibrugarh University, Dibrugarh-786004, Assam, India; paribgo4@gmail.com (P.B.);
[2] Department of Chemistry, DUIET, Dibrugarh University, Dib[1]rugarh-786004, Assam, India; Email: gitaleesharma@dibru.ac.in (G.S.);
[3] DGM, OGPL & P, Oil India Limited, Duliajan, Duliajan-786602, Assam, India; prankush@oilindia.in (P.M.B.);
[4] Chief Chemist, Chemical Department, Oil India Limited, Duliajan, Duliajan-786602, Assam, India; uddipanas_deka@oilindia.in (U.S.D.);
[5] DGM, Chemical Department, Oil India Limited, Duliajan, Duliajan-786602, Assam, India; dipakjkalita@oilindia.in (D.J.K.);
* Correspondence: gitaleesharma@dibru.ac.in (G.S.);

Scopus Author ID 57211854016
Received: 14.08.2022; Accepted: 19.09.2022; Published: 31.10.2022

Abstract: CO_2 corrosion has emanated as a significant concern in the oil/gas industry owing to the aging of its oilfields. Thus, corrosion protection is significant for maintaining the integrity and sustainability of pipelines, surface facilities, and downhole tools in the oil/gas sector. The present study evaluates the corrosion inhibitory properties of three oxazolone derivatives in CO_2 saturated 3.5 weight% NaCl solution against API5LX60 carbon steel used in certain wells and oil/ gas transportation pipelines. The inhibitory behavior was investigated utilizing gravimetric and electrochemical techniques viz. EIS, PDP, and LPR. Electrochemical and Gravimetric technique results were in congruence. EIS asserts capacitive behavior, and PDP affirms oxazolones as mixed inhibitors. SEM and SEM-EDX confirmed the formation of a protective layer by adsorption. At an optimum inhibitor concentration of 200 ppm, inhibitor I exhibited 91.30% inhibition—linear correlation coefficient R^2 value of 0.99 avowed adsorptions via Langmuir Isotherm.

Keywords: API5LX60 carbon steel; oxazolone; EIS; SEM-EDX; corrosion inhibition.

1. Introduction

Corrosion caused by CO_2 is a serious hazard to certain wells and crude oil transportation pipelines of oil/ gas industries around the globe [1]. API5LX60 steel is extensively used in these pipelines due to its versatility and ease of supply. CO_2/H_2O is pumped into oil wells to boost crude oil production, making it even more corrosive to carbon steel [2]. CO_2 in its dry state is not corrosive, but the aqueous solution gives it corrosive property. Although the specific process is unknown, it is assumed that dry CO_2 is transformed into carbonic acid in an aqueous environment [3, 4].

Corrosion inhibitors have been used for ages as preventive measures against corrosion attacks of aggressive media [5, 6]. However, inorganic inhibitors, being hazardous, have limitations over organic inhibitors [7]. Organic inhibitors with chromophores and auxochromes

such as derivatives of amino acids, 3.4-diaminobenzonitrile, mycophenolic acid, oxadiazole, quinolines, imidazolines, amido-imidazoline, azoles, pyrimidine, benzenesulphonamide, dodecylbenzenesulphonamide, polythiazole, imidazoline-thione, thiols, poly aspartic acid, imidazole-pyridine, etc. inhibit corrosion effectively as they establish positive adsorption on steel surface forming a protective layer which shields the material from corrosive medium [8-23]. Nanomaterials also show significant inhibitive properties [24].

Oxazolones are excellent bioabsorbable, sustainable organic compounds with a wide range of therapeutic actions and anticorrosive properties [25, 26]. In this work, three oxazolone derivatives, namely 2-Methyl-4-naphthalen-2-ylmethylene-4H-oxazol-5-one (I), 4-(2-Methyl-5-oxo-oxazol-4-ylidenemethyl)-benzaldehyde (II) and 4-(2-Methyl-5-oxo-oxazol-4-ylidenemethyl)-benzene (III) were synthesized from procedures noted in the literature [27-30]. Gravimetric weight loss coupons and electrochemical techniques viz. Electrochemical Impedance Spectroscopy (EIS), Potentiodynamic Polarization Measurement (PDP), and Linear Polarization Resistance (LPR) were employed in the evaluation of CO_2-saturated 3.5 weight % NaCl solution with four varieties of inhibitor concentrations. Surface morphology studies viz SEM and SEM-EDX were conducted on the API5LX60 steel samples before and after inhibitor coating. Test solutions were examined via UV-visible spectroscopy. Further, the results obtained were allowed to fit on the adsorption isotherm.

2. Materials and Methods

2.1. Inhibitor synthesis and electrochemical measurement.

The three oxazolone derivatives were synthesized as depicted in Scheme 1 [27-29].

Steel coupons of dimension 3.8cm x 1.0 cm x 0.8 cm and exposed surface area 0.8 cm^2 were employed for the electrochemical measurements. The steel coupons were polished with emery papers, washed with double distilled water, degreased with acetone, and dried at 60-70^{0}C. The API5LX60 carbon steel composition studied herein is depicted in Table 1. The test solution of 3.5-weight % NaCl was prepared using analytical grade NaCl with double distilled water, which was saturated with CO_2 at a pressure of 700kPa. For the weight loss studies, the steel coupons were left to stand unfettered in the trial solution in uninhibited conditions at room temperature (25-28^{o}C) for 24 hours. Coating the coupons with four concentrations (50,100,150,200 ppm) of the three inhibitor molecules was done, and a similar procedure was adopted. The minimum and maximum concentrations were chosen at 50 ppm and 200 ppm, respectively (as a number of literature pieces were in line with this surmise). Over the 200 ppm mark, the weight reduction outcomes were comparable. Eventually, the optimal concentration was stabilized at 200 ppm.

Percentage Inhibition efficiencies (%IE) for different inhibitor concentration was evaluated from weight loss difference before and after the addition of inhibitor to the steel specimens using equation (1) [3]:

$$\%IE = \left(1 - \frac{\Delta W_i}{\Delta W}\right) \times 100 \quad (1)$$

where ΔW= average weight loss in uninhibited condition, and ΔW_i= average weight loss in inhibited condition.

Equation (2) is employed for corrosion rate (CR) calculations [3]:

$$Corrosion\ Rate = \frac{8.76 \times 10^6 \times \Delta W}{a \times t \times d} \quad (2)$$

where the quantity ($8.76X10^4$) allows to represent corrosion rate in mm/yr; a = surface of metal sample (in cm^2); t = immersion time (hours); d = metal's density (g/cm^3); ΔW = average weight loss (g).

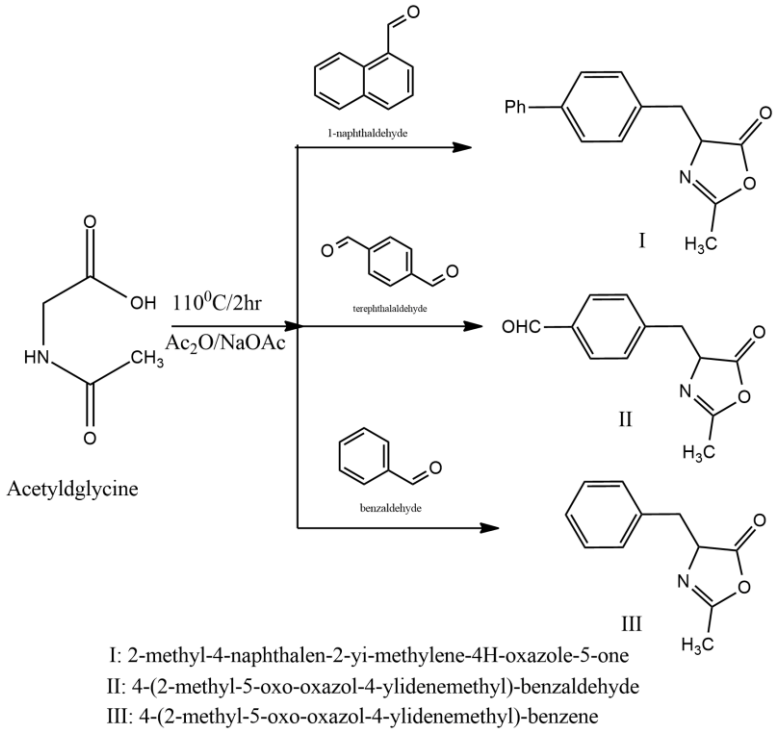

Scheme 1. The three oxazolone derivatives were synthesized, as represented in Scheme 1. A mixture of acetylglycine (10g,0.085mol), aromatic aldehyde {1-naphthaldehyde (4.5ml,0.0288 mol) or terephthaldehyde (1g, 0.0075mol), or benzaldehyde (4mL, 0.0376mol)}, sodium acetate (5g, 0.06mol) and acetic anhydride (5ml,0.04897mol) were refluxed at 110^0C for 2 hours. TLC was checked (in 20% ethyl acetate/hexane) to check the progress of the reaction. After 2 hours single spot observed, confirming product formation. The product was recrystallized with 30:70 ethyl acetate and hexane. The synthesized inhibitors' purity was checked using TLC in 20% ethyl acetate/hexane solvent. FTIR spectra of the inhibitor compounds in the solid state were recorded using SHIMADZU IRAffinity-1 Spectrophotometer. ^{1}H and ^{13}C NMR were recorded using TMS as an internal standard. All the solvents used were deuterated. Melting points were recorded using the melting point apparatus. 2-Methyl-4-naphthalen-2-ylmethylene-4H-oxazol-5-one (I): Orange powder; Yield 95%; m.p. 116-118 ^{o}C: ^{1}H NMR (400 MHz, $CDCl_3$): δ 2.5 (s, 3H, CH_3), 7.32 (dd, J = 8.6, 2H, ArH), 7.6 (d, J = 7.8,1H, ArH), 7.9 (s, 1H, =CHAr), 8.0 (d, J = 8.0, 1H. ArH), 8.3 (d, J = 8.4, 2H, ArH), 8.8(s, 1H, ArH). ^{13}C NMR (400 MHz, $CDCl_3$): δ 168, 167, 136.3, 133.8, 133, 132, 131, 129, 127, 126.5, 126, 125, 124, 121, 78; IR (KBr, γ/cm^{-1}): 3952, 3650, 3526, 3360, 3256, 3041, 2649, 2465, 2330, 2154, 2066.4-(2-Methyl-5-oxo-oxazol-4-ylidenemethyl)-benzaldehyde (II): Red powder; Yield 92%; m.p. 118-120 ^{o}C: ^{1}H NMR (400 MHz, $CDCl_3$): δ 2.5 (s, 3H, CH_3), 7.2 (s, 1H, =CHAr), 7.8(d, J = 8.4, 2H, ArH), 8.0 (d, J = 8.6, 1H, ArH), 9.5(d, J = 8.6, 1H, ArH), 10(s, 1H, CHO); ^{13}C NMR (400MHz, $CDCl_3$): δ 192, 169, 167, 141, 136, 135, 131, 130.5, 127, 126.7,126.6, 78; IR:(KBr: γ/cm^{-}1)3946, 3849, 3059, 2360, 1958, 1790. 4-(2-Methyl-5-oxo-oxazol-4-ylidenemethyl)-benzene (III): Yellow powder; Yield 90%; m.p.110-112 ^{o}C: ^{1}H NMR (400 MHz, $CDCl_3$): δ 2.5 (s, 3H, CH_3), 7.2 (s, 1H, =CHAr), 7.3(dd, J = 7.6, 1H, ArH), 7.5 (dd, J = 7.8, 2H, ArH), 8.1(d, J = 8.2, 2H, ArH); ^{13}C NMR (400 MHz, $CDCl_3$): δ 175, 165, 136.3, 132, 131.5, 131, 129, 127.7, 126.6, 126.6, 76; IR: (KBr: γ/cm^{-}1)3946, 3849, 3058, 2359, 1958, 1790, 1034, 562, 406 [26, 27].

Table 1. Composition of steel sample.

Element	C	Mn	P	S	V	Nb	Ti	Fe
Wt %	0.28	1.4	0.3	0.3	≤15	≤15	≤15	Balanced

Electrochemical measurements at room temperature were conducted using a Metrohm Autolab Potentiostat/Galvanostat PGSTAT302N with ASTM G-59 and ASTM G-102 standard protocol [30]. A three-electrode system with an Ag/AgCl electrode, stainless steel (SS316)

electrode, and the cold-mounted steel specimen with an exposed area of 1cm^2 was the reference, counter, and working electrode, respectively. To maintain a constant Open Circuit Potential (OCP), the working electrode was submerged in electrolyte for 30 minutes. The Potentiostatic Electrochemical Impedance Spectroscopy (EIS) was done at an amplitude of ±10mV and a frequency sweep of 10 mHz to 100 kHz. The equivalent circuit model fit the EIS spectra shown in Figure 1. The model was drawn using the parameters - solution resistance (R_s), polarization resistance (R_p), constant phase element (CPE), and phase shift (n). These parameters were obtained as curve fittings' results. The equation below gives the impedance of the CPE [31]:

$$Z_{CPE} = Y_0^{-1}(i\omega)^{-n}$$

where the magnitude of CPE is Y_0, angular frequency ω, and phase shift n.

The % Inhibition Efficiency from EIS measurements can be done using the equation [31]:

$$\%EIS = \left(1 - \frac{R_p}{R_p^I}\right) \times 100\%$$

where R_p and R_p^I are the polarization resistances of the solutions with uninhibited and inhibited samples respectively. R_p is the sum of R_f (film resistance) and R_{ct}(charge transfer resistance). Double layer capacitance (C_{dl}) values were calculated using the equation at the frequency where the imaginary component of the spectrum (I_{max}) is maximal:

$$C_{dl} = \frac{1}{2\pi I_{max} R_{ct}}$$

LPR was measured at a potential realm of ±10mV from OCP at 0.125mV/s scan rate. LPR is a quick, non-destructive electrochemical measurement technique commonly employed to get corrosion rates of materials [32]. In this approach, corrosion current and potential may be linearly correlated by a slight polarization of about ±10 mV relative to OCP. The LPR parameters were tabulated from data obtained from curve fitting. Further, PDP was performed at about ±250mV potential range from OCP and 0.25mV/s sweep rate. PDP measurements are a destructive approach that uses a comparatively larger potential range of 200 to 400 mV. This approach provides us with more information than LPR. PDP data analysis is utilized for electrochemical processes to assess the impact of inhibitors. For data analysis and curve fitting, Nova Software was employed.

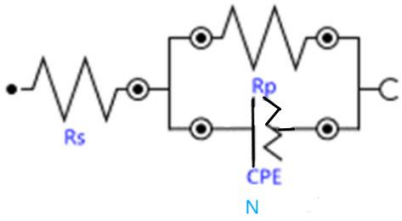

Figure 1. Equivalent circuit model of electrochemical studies.

2.2. Test solution and surface characterization.

The samples were subjected to UV-Visible detection using SHIMADZU UV-Visible Spectrophotometer (Model UV1900) with a wavelength range of 200-800 nm, medium scan rate, and light source λ= 340.8 nm. The steel coupons were plunged in different test solution

concentrations in inhibited and uninhibited conditions and allowed for room temperature drying. The samples micrographs were taken with FESEM instrument Model Sigma. SEM Energy Dispersed X-ray Spectroscopic (SEM-EDX) technique (using FESEM Instrument (Model Sigma)) detected the elemental composition of the samples before and after dousing in the electrolyte. The gold coating was done at "Timed Gold" mode with a sputtering current of 20mA and sputtered time of 59 seconds.

3. Results and Discussion

3.1. Weight–loss measurements.

In the gravimetric technique, all the measurements were performed in triplicate, and the average weight loss values yielded corrosion rates and inhibition efficiencies. The outcomes are tabulated in Table 2. Observations made from Table 2 results report showed a drastic inhibition efficiency increase on the application of inhibitor compounds. Corrosion rates reduced as inhibitor concentration increased for all three inhibitors. The % Inhibition efficiency seems to be higher in the case of compound I with respect to compounds II and III, implying greater adsorption of compound I on steel surface than compounds II and III. The increased adsorption is due to the presence of heteroatoms O and N in the oxazolone molecules, which form coordinate bonds with the metal surface. Conjugation in the oxazolones is another reason for their increased % inhibition efficiencies. The corrosion rate and inhibition efficiency changes with concentration variation can be explained more precisely in Figure 2, shown below. Figure 2 (a) displays increased inhibition efficiency with concentration increase for Inhibitor I. Similar is the case with Inhibitors II and III. Figure 2(b) establishes the corrosion rate decrease after the inhibitor applies for all three cases. The corrosion rate further decreased as inhibitor concentration exceeded, which is optimized at 200 ppm; above it the corrosion rate variation remained constant.

Table 2. Weight loss measurements of the working samples; *IC=Inhibitor Concentration, CR=Corrosion Rate, IE=Inhibition Efficiency.

Sample	***IC (in ppm)***	***Wt. loss (in g)***	***CR (mmpy)***	***%IE***
Steel coupon with Inhibitor I	0	0.23	13.36	0
	50	0.11	6.393	52.17
	100	0.09	5.23	60.86
	150	0.05	2.90	78.26
	200	0.02	1.16	91.30
Steel coupon with Inhibitor II	0	0.23	13.36	0
	50	0.13	7.56	43.47
	100	0.10	5.81	56.52
	150	0.09	5.23	60.86
	200	0.04	2.32	82.60
Steel coupon with Inhibitor III	0	0.23	13.36	0
	50	0.14	7.30	39.13
	100	0.11	6.39	52.17
	150	0.07	4.06	69.56
	200	0.05	2.90	78.26

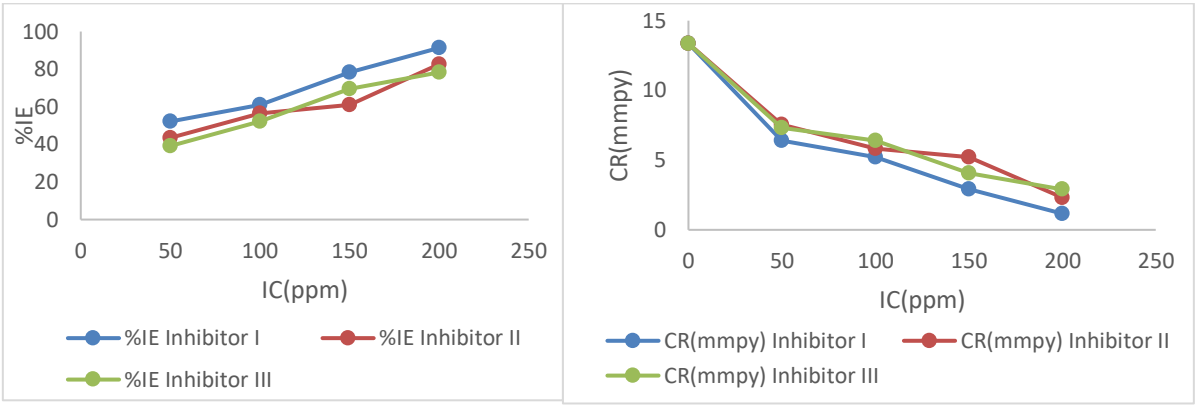

(a) **(b)**

Figure 2. (a) % Inhibition efficiencies vs. inhibitor concentration; **(b)** Corrosion rate vs. inhibitor concentration for all three inhibitors.

3.2. EIS measurements.

The Nyquist, Bode, and Bode modulus plots observed for the uninhibited and the prototype oxazolone (I) inhibited solutions are exhibited in Figures 3(a), 3(b), and 3(c). The Nyquist plots were specified by semi-circular arcs that indicate capacitive character. These arcs are represented by two-time constants, one at high frequency and the other at low-frequency regions in the Bode plots. The creation of an adsorption layer on API5LX60 steel surface is represented by the high-frequency region time constant, viz. R_f//CPE_f., where R_f is film resistance and $CPE_{f,\,is}$ the Constant Phase Element for film formation. Conversely, an electrical double-layer formation at the electrode-electrolyte interface is portrayed by the time constant at low-frequency region, viz. R_{ct}//$CPE_{dl,}$ where charge transfer resistance is R_{ct} and CPE_{dl} is double layer Constant Phase Element [33, 34].

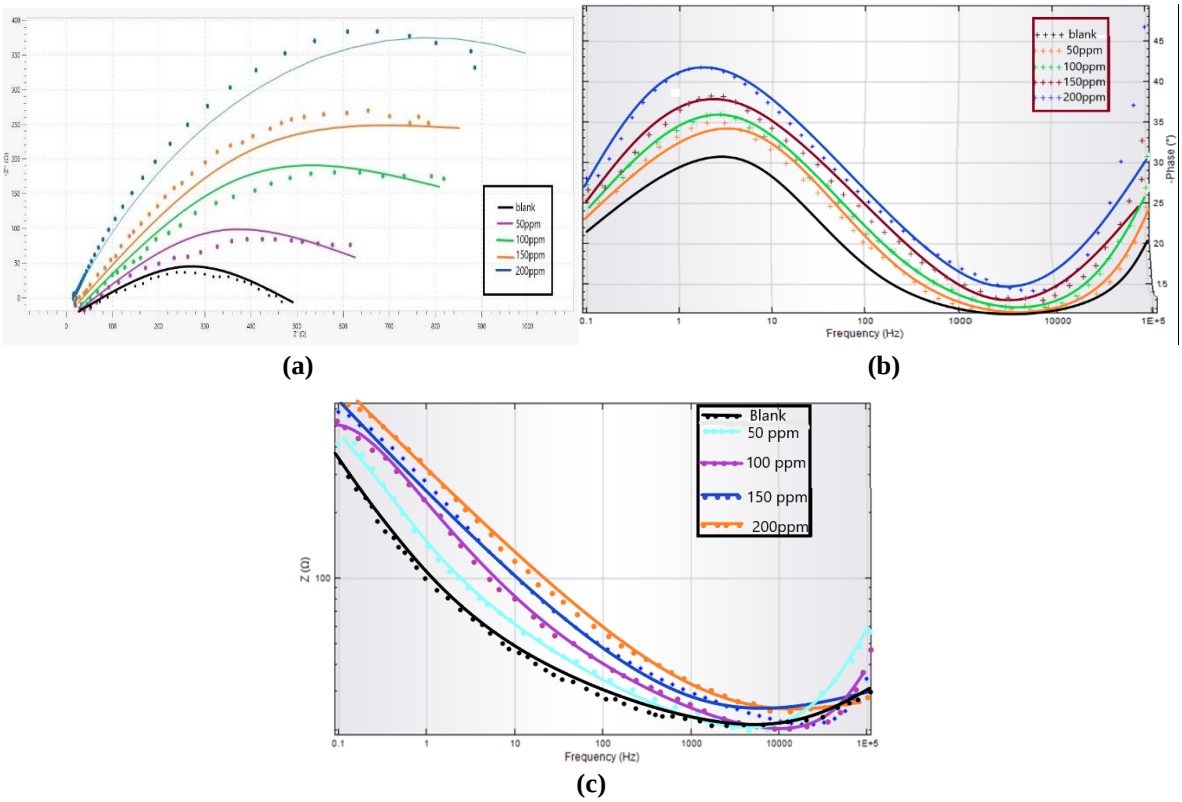

(a) **(b)**

(c)

Figure 3. (a) Nyquist plots; **(b)** Bode phase plots; **(c)** Bode modulus plots for Inhibitor I at different concentrations.

The distortion in the semi-circles of Nyquist plots may occur thence the presence of some impure substances and deformities on the API5LX60 surface (as the steel sample taken was the corroded used one from the transmission pipelines of an oil industry). The diameter of the semi-circular arc for the inhibited solutions was greater than the uninhibited one.

Table 3. EIS data for the oxazolone inhibitors.

Solution	Conc. of Oxazolone	Fitted Z' (Ω)	Angle vs. X axis	CPE.Y0 (F)	Rp.R (Ω)	Rs.R (Ω)	CPE.N	%IE
Uninhibited	0	25.912	-0.612	0.00042	377.42	46.78	0.99201	-
Inhibitor I	50	20.577	-0.631	0.00078	719.34	14.94	0.99277	47.53
	100	18.668	-0.660	0.00082	996.87	13.50	0.99452	62.14
	150	23.364	-0.314	0.00117	1360.00	83.22	0.99612	72.25
	200	24.130	-0.515	0.00185	1855.00	68.14	0.99894	79.65
Inhibitor II	50	22.121	-0.472	0.00049	654.36	23.46	0.99032	42.32
	100	37.329	-0.742	0.00108	1064.05	30.68	0.99144	64.53
	150	26.832	-0.543	0.00392	1253.05	35.78	0.99543	69.88
	200	21.979	-0.188	0.00432	1671.48	46.41	0.99763	77.18
Inhibitor III	50	25.571	-0.342	0.00042	975.98	80.74	0.99063	61.33
	100	23.592	-0.506	0.00153	1043.80	41.76	0.99401	63.84
	150	20.979	-0.554	0.00232	1205.50	55.53	0.99534	68.69
	200	54.433	-0.372	0.00473	1514.30	74.64	0.99613	75.08

This increase in diameter is allocated to creating a protective layer on the metal surface against corrosive media (electrolyte), thereby amplifying carbon steel resistance to corrosion [35]. With inhibitor concentration increase, the diameter of the semi-circular arc increases and was highest for 200 ppm inhibitor concentration, which suggests that inhibition efficiency is directly related to inhibitor concentration. Similar plots are obtained for both inhibited and uninhibited solutions, suggesting that the corrosion mechanism remains unchanged despite the decrease in corrosion rate for an inhibited solution. The oxazolone molecules got adsorbed on the API5LX60 steel surface by creating a coordinate covalent bond between the surface of steel and heteroatoms, thereby forming a protective layer and preventing corrosion attacks on the steel surface. The Bode phase plots' diameter surged after the inhibitor application, owing to a similar explanation as the Nyquist plots. In Bode modulus plots, the linear part for the intermediate frequency range is relatively more evident for inhibited solutions and reaches a maximum of 200 ppm inhibitor concentration.

The R_p values for the inhibited solutions escalated owing to the oxazolone molecules' steel surface protective coating formation. This further prevents the surface from corrosive attack and the transfer of charge and mass from it. The solution resistance (R_s) values were also elevated for inhibited solutions. The corrosion data attained from EIS measurements are outlined in table 3 above. Although there is a difference in % IE values obtained from gravimetric analysis and EIS measurements, both studies agree that % IE is concentration dependent and highest for Inhibitor I.

3.3. LPR measurements.

Table 4 below depicts the LPR results. The E_{corr} values obtained from LPR measurements for inhibited solution were less negative than the uninhibited one, although there was no regular trend of E_{corr} values with varying inhibitor concentrations. This suggests that oxazolone act as a mixed/ hybrid type of inhibitor by inhibiting redox reactions on carbon steel. The current density j_{corr} showed an increase in its values with concentration enhancement. The

increase in oxazolone inhibitor concentration in all cases provoked high corrosion current densities and hence high cathodic and anodic activities. The % Inhibition efficiency from LPR measurements was calculated using the formula given below [34]:

$$\%IE_{LPR} = \left(1 - \frac{R_P}{R_p^I}\right) \times 100\%$$

The %IE also exceeded with inhibitor concentration reaching the highest at 200 ppm concentration. Again, the smaller χ^2 statistics revealed that the observed data fit the expected data extremely well. The extent of fitting was best with 200 ppm inhibitor concentration, and for all three oxazolones, the order of best-fit upsurges with a rise in the inhibitor concentration. The lowest χ^2 statistics were observed at 200 ppm inhibitor concentration for all three inhibitors. Thus, the concentration dependence of the LPR parameters affirms that the LPR measurement results were in congruence with the gravimetric analysis.

Table 4. Linear Polarization Resistance studies data for oxazolone inhibitors.

Solution	Concentration (ppm)	Ecorr (V)	jcorr (μA/cm²)	Polarization resistance (Ω)	χ^2 ($x10^{-10}$)	%IE
Uninhibited	0	-0.494	0.000185	205.27	0.107	--
Inhibitor I	50	-0.466	0.000046	392.51	0.033	47.70
	100	-0.548	0.000047	445.73	0.024	53.95
	150	-0.476	0.000165	781.15	0.018	73.72
	200	-0.472	0.000175	1467.2	0.001	86.01
Inhibitor II	50	-0.498	0.000043	383.96	0.089	46.54
	100	-0.491	0.000045	461.09	0.069	55.48
	150	-0.492	0.000250	581.95	0.003	64.73
	200	-0.470	0.000301	788.01	0.002	73.95
Inhibitor III	50	-0.529	0.000016	359.85	0.067	42.95
	100	-0.566	0.000041	444.58	0.088	53.82
	150	-0.493	0.000065	468.00	0.004	56.14
	200	-0.478	0.000149	663.03	0.0008	69.04

3.4. PDP measurements.

Figure 4 displays the PDP plots acquired during measurement. The inhibited solutions' cathodic current density reduced significantly compared to the uninhibited solutions, indicating that inhibitor addition blocked some cathodic processes. Again, the current density j_{corr} showed an increase in its values with concentration surge, similar to the case of all three inhibitors. This observation implies that an increase in oxazolone inhibitor concentration incited high corrosion current densities, hence high cathodic and anodic actions. Similarly, the E_{corr} values for inhibited solutions went toward less negative. However, there were no consistent correlations between E_{corr} values and inhibitor concentration, suggesting that the used inhibitor is a hybrid [36]. Table 5 displays the result of Tafel fit with parameters viz. corrosion potential (E_{corr}), corrosion current (I_{corr}), anodic Tafel slope (βa), cathodic Tafel slope (βc), and corrosion rates. Also, when inhibitor concentration increased, I_{corr} values fell, reaching a nadir at 200 ppm. Based on PDP data, the effectiveness of inhibition was determined using the succeeding equation [36]:

$$\%IE_{PDP} = \left(1 - \frac{I^{I}_{corr}}{I_{corr}}\right) \times 100\%$$

where I^{I}_{corr} and I_{corr} are the densities of corrosion current for both inhibited and uninhibited samples. The inhibited solutions' I_{corr} values were much lower, considering protective inhibitor film formation. I_{corr} readings similarly reduced as inhibitor concentration increased. However, inhibition efficiencies rose as inhibitor concentration exceeded. The % IE and corrosion rates calculated by PDP and gravimetric methods were parallel. In both instances, raising the inhibitor concentration decreases the corrosion rate and raises the proportion of inhibited corrosion, i.e., % inhibition efficiency. Hence it validates both gravimetric and electrochemical measurements.

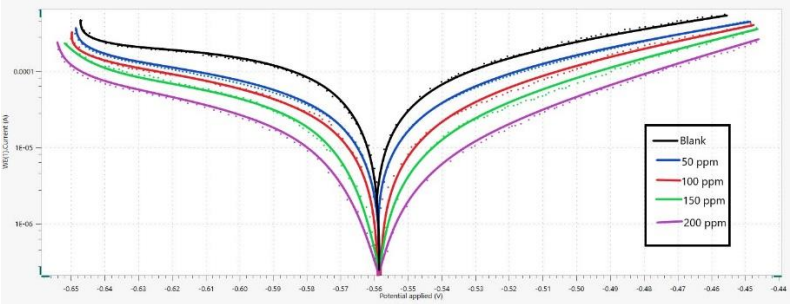

Figure 4. Tafel plots for inhibitor I at different concentrations.

Table 5. Corrosion data obtained from potentiodynamic polarization studies.

Solution	Concentration (ppm)	βa (V/dec) (V/dec)	βc (V/dec) (V/dec)	Ecorr, (V)	jcorr (A/cm²) (A/cm²)	Icorr (A) (A)	Corrosion rate (mm/ year)	χ^2 ($x10^{-11}$)	%IE
Uninhibited	0	0.1059	0.2609	-0.4979	0.000185	0.000159	2.15	1.07	--
Inhibitor I	50	0.0445	0.1030	-0.5661	0.000041	0.0000393	0.48	0.211	75.28
	100	0.0488	0.1254	-0.49272	0.000060	0.0000262	0.35	0.038	83.52
	150	0.0851	0.1716	-0.4729	0.000175	0.0000168	0.20	0.012	89.43
	200	0.0726	0.2112	-0.5297	0.000183	0.0000147	0.19	0.006	90.75
Inhibitor II	50	0.0531	0.1234	-0.4651	0.000046	0.0000411	0.54	0.180	74.15
	100	0.0411	0.1275	-0.4947	0.000066	0.0000288	0.40	0.044	81.88
	150	0.0521	0.1356	-0.5141	0.000115	0.0000230	0.35	0.041	85.52
	200	0.0412	0.0837	-0.4760	0.000165	0.0000154	0.19	0.033	90.31
Inhibitor III	50	0.0523	0.1199	-0.4993	0.000043	0.0000412	0.57	0.892	74.08
	100	0.0291	0.0789	-0.5493	0.000047	0.0000375	0.55	0.235	76.41
	150	0.0913	0.2101	-0.4785	0.000149	0.0000323	0.50	0.089	79.65
	200	0.0608	0.1776	-0.4709	0.000250	0.0000250	0.29	0.002	84.28

3.5. SEM and SEM-EDX.

Micrographs obtained from scanning electron microscopy analysis are specified in Figure 5(a), 5(b), 5(c), and 5(d). Figure 5(a) depicts the morphology of an uninhibited corroded API5LX60 steel surface having deformity due to the corrosive attack of an acidic environment. Figure 5(b) is for API5LX60 steel surface coated with inhibitor I at 200 ppm concentration, and 5(c) and 5(d) are for API5LX60 steel with inhibitor II and III, respectively, at 200 ppm

concentration. It was discovered that the steel surface appeared to be flat and smooth as an outturn of the steel surface's adsorption by the inhibitor and subsequent forming of a protective coating.

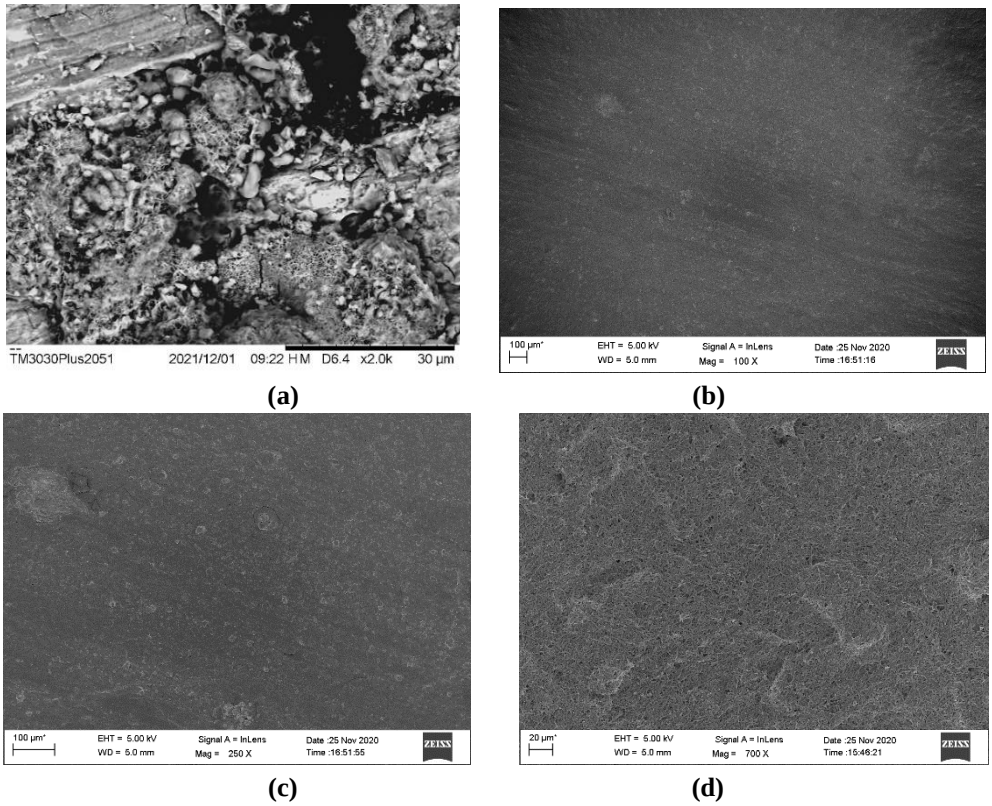

Figure 5. (a) SEM micrograph for uninhibited steel; **(b)** SEM micrograph for API5LX60 steel coated with inhibitor I; **(c)** SEM micrograph for API5LX60 steel coated with inhibitor II; **(d)** SEM micrograph for API5LX60 steel coated with inhibitor III.

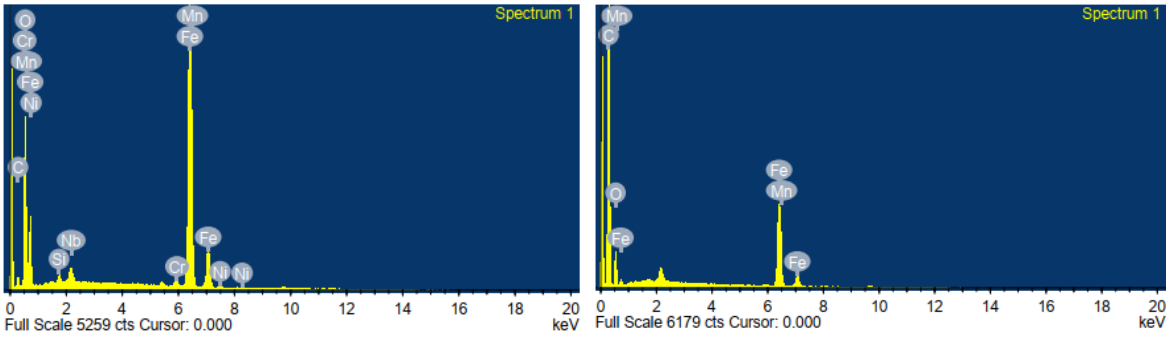

Element	Weight %	Atomic %
C K	4.18	11.21
O K	23.94	48.15
Si K	0.60	0.69
Cr K	0.45	0.28
Mn K	1.00	0.59
Fe K	66.03	38.04
Ni K	0.78	0.43
Nb L	0.73	0.25
Au M	2.28	0.37

Figure 6 (a). SEM-EDX Spectrum for Uninhibited steel.

Element	Weight %	Atomic %
C K	64.03	81.24
O K	13.84	13.18
Mn K	0.24	0.07
Fe K	19.53	5.33
Au M	2.36	0.18

Figure 6 (b). SEM-EDX spectrum for Inhibited steel with prototype Inhibitor I.

The spectrum obtained from SEM-EDX spectrum imaging is depicted in figure 6 below with elemental composition. Figure 6(a) refers to the spectrum of uninhibited steel surfaces, while figure 6(b) refers to the spectrum of inhibited API5LX60 steel surfaces with prototype Inhibitor I of 200 ppm concentration. The SEM-EDX spectra of constituent elements reveal that the percentage of carbon and oxygen increased for the API5LX60 steel sample coated with inhibitor I, implying efficient coating of inhibitor compound on the steel surface. Similar observations were noted for steel coated with inhibitors II and III. The percentage composition of carbon and oxygen increased, whereas that of iron and other metals decreased in the inhibitor-coated steel, thereby suggesting the formation of an effective inhibitive layer of the synthesized oxazolone molecules.

3.6. UV-visible studies.

UV-Visible studies were performed for the test solutions in both conditions before and after immersion of steel samples. The UV-Visible studies exhibited that the λ_{max} of the test solutions with inhibitor-coated samples surged due to the slight decomposition of the coated inhibitors in it. Spectra attained for 3.5% NaCl solution with CO_2 saturation in both conditions with varying concentrations of inhibitors I, II, and III are depicted in Figures 7(a), 7(b),7(c), and 7(d) below.

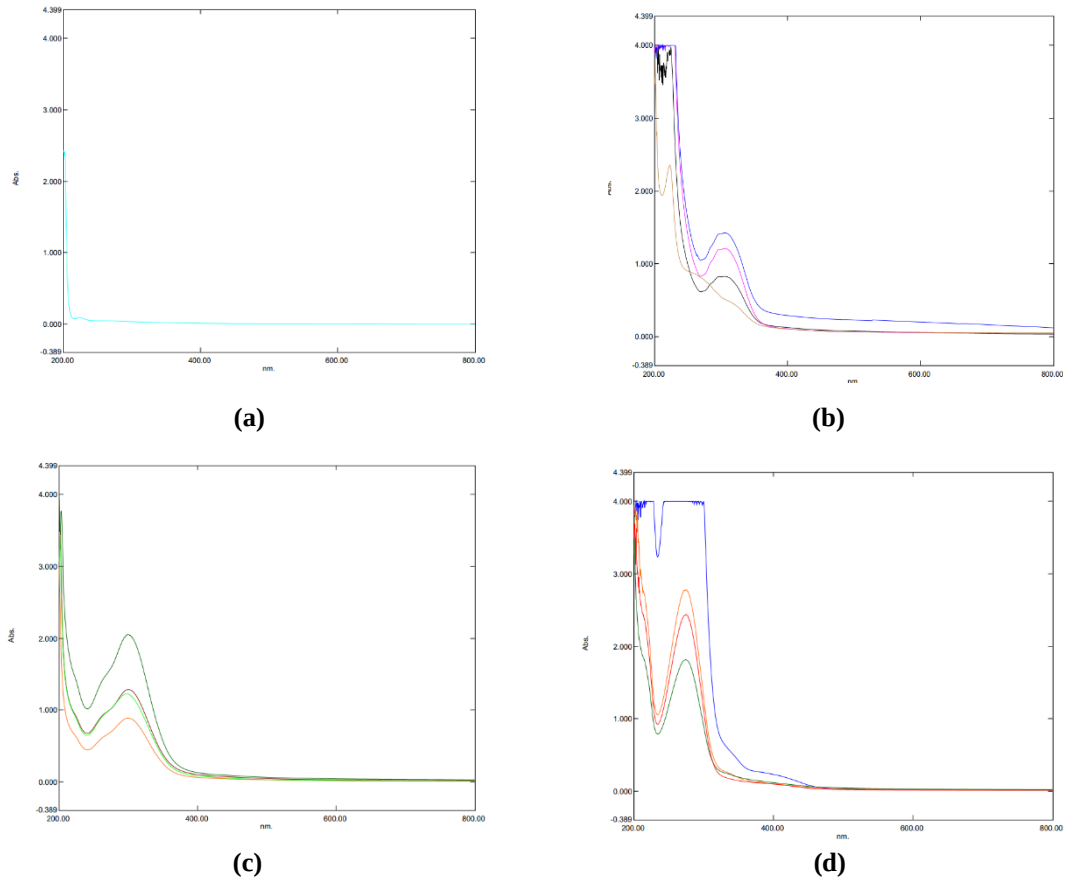

Figure 7. (a) UV-Visible Spectra for uninhibited 3.5% NaCl+CO_2; **(b)** Spectra for test solution with Inhibitor I; **(c)** Spectra for test solution in Inhibitor II; **(d)** Spectra for test solution in Inhibitor III.

3.7. Mechanism of inhibition.

Conjugated systems of π--electrons and heteroatoms in organic molecules have an inhibitory effect attributable to the inhibitors' adsorption by the foundation of a metal-inhibitor complex on the steel surface via a connection between metal and the single electron present in

inhibitor compounds [37]. In addition to the production of the Fe-oxazolone complex, oxazolone molecule adsorption on the electrode-electrolyte interface may be employed to explain the inhibitory effects of the specified inhibitor. Figure 8 displays the creation of an adsorbed layer at the boundary between the ferrous ion (from API5LX60 steel) and the oxazolone inhibitor molecule. Thus, it may be extrapolated that the metal-inhibitor adsorbed combination produced a shield on the surface of the API5LX60 steel, thereby protecting it from additional electrolyte corrosion.

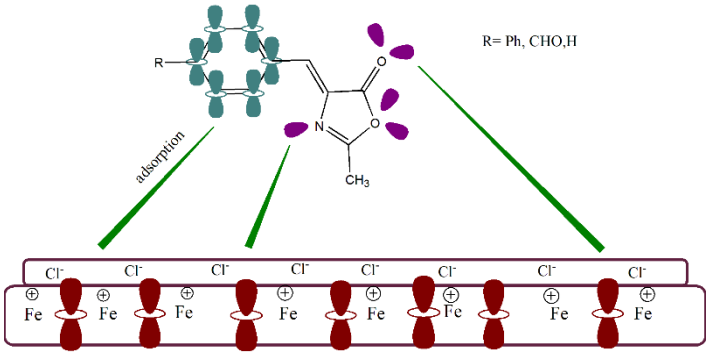

Figure 8. Mechanism of API5LX60 steel inhibition by oxazolone derivatives.

3.8. Langmuir adsorption isotherm.

It is expected that adsorption occurring on the surface of the steel, acts as a protective barrier and limits the hostile medium's corrosive attack. The kind of adsorption may be physical, chemical, or both. Using experimental data derived from weight loss and electrochemical tests, the adsorption behavior of oxazolone derivatives on API5LX60 steel surface was investigated. Among the many isotherms of the Tempkin, Langmuir, and Freundlich models, the experimental results best suited the Langmuir adsorption isotherm. This isotherm is a plot of log C/θ versus log C, and its formula is provided below in the equations below [38]:

$$C/\theta = 1/K_{ads} + C$$

$$\theta = \%IE/100$$

where, the surface coverage is θ, the concentration of inhibitor C, and adsorption equilibrium constant K_{ads}, the values of K_{ads} as calculated from (1) has been tabulated in table 6. It is acclaimed that in order for an inhibitor to conform to the Langmuir isotherm, its linear correlation coefficient (R^2) must equal one. Figure 9 shows a plot of C/ θ against C for inhibitor I, which is a straight line with a slope almost equal to 1 and R^2 values of the order 0.99, as reported in table 6. Thus, it confirms the Langmuir adsorption behavior of the oxazolone derivatives on the API5LX60 steel surface.

Gibb's free energy of adsorption is linked to K_{ads} by the equation presented below:

$$\Delta G^0_{ads} = -RTln(1 \times 10^6 K_{ads})$$

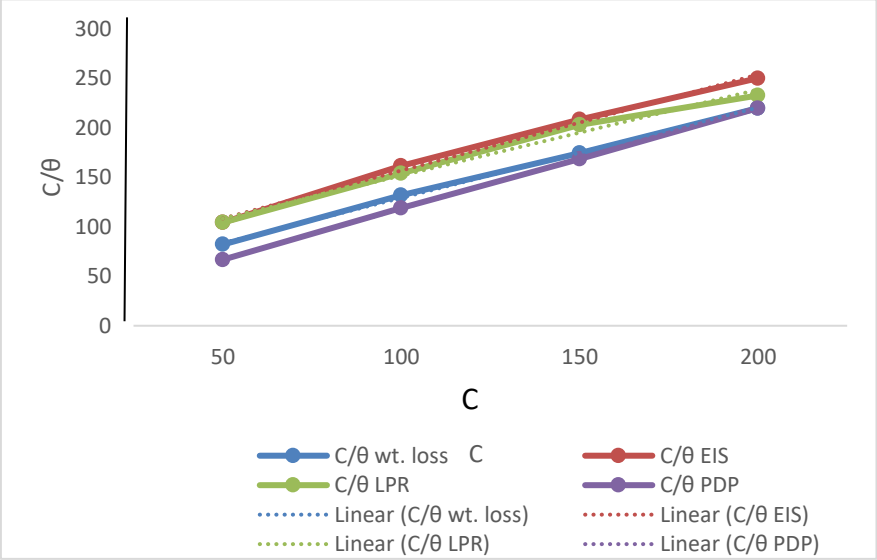

Figure 9. The plot of C/θ Vs C for inhibitor I.

Table 6. Adsorption data obtained from gravimetric and electrochemical studies**.**

Method	IC (ppm)	%IE	θ	R^2	K_{ads}(ppm)	ΔG^0_{ads}(kJ/mol)
Weight loss	50	61.06	0.61	0.999	0.0264	-25.224
	100	76.10	0.76			
	150	86.28	0.86			
	200	90.70	0.91			
EIS	50	47.50	0.48	0.995	0.0167	-24.089
	100	62.14	0.62			
	150	72.24	0.72			
	200	79.65	0.80			
LPR	50	47.70	0.48	0.988	0.0154	-23.889
	100	64.65	0.65			
	150	73.72	0.74			
	200	86.00	0.86			
PDP	50	75.28	0.75	0.999	0.0613	-27.311
	100	83.52	0.84			
	150	89.43	0.89			
	200	90.75	0.91			

Usually, when ΔG^0_{ads}values for adsorption have a maximum of -20 kJ/mol; the mechanism is physisorption. On the contrary, if ΔG^0_{ads} has a value greater than -40kJ/mol, and adsorption is believed to occur through a chemisorption mechanism via the formation of a coordinate covalent bond [36-38]. ΔG^0_{ads} values obtained from the gravimetric and other electrochemical data range from -27.311 to -23.889, which is indicated in table 6. These negative values imply that the oxazolone adsorption onto the API5LX60 steel surface is spontaneous and proceeds via the physisorption mechanism as the ΔG^0_{ads} values are in close proximity to the physical adsorption range.

4. Conclusions

Oxazolone's biocompatible, environmentally benign, and medicinal qualities prompted this study into its use as a corrosion inhibitor in oil wells and transmission pipelines. This report synthesized three oxazolone derivatives with good anticorrosion properties for API5LX60 steel used in the oil and gas sectors. A CO_2-saturated 3.5 % NaCl solution was used as the experimental medium. At 200 ppm concentration, inhibitor I exhibited the highest inhibitory effectiveness, which was 91.30 % in weight loss experiments and 90.7 % according to electrochemical investigations (PDP). In addition, corrosion rates decreased as the inhibitor

concentration rose, resulting in an improvement in inhibition efficiency. Both weight loss measures and electrochemical investigations were in congruence as they emphasized the inhibitor concentration dependence of % inhibition efficiency. The corrosion process's capacitive character has been validated by EIS measurements. Polarization resistance tests on trial materials divulged that the synthesized molecules behaved as a mixed kind of inhibitor. Furthermore, SEM and SEM-EDX analyses implied the creation of a protective inhibitor film on the API5LX60 steel surface by adsorption. Adsorption thermodynamic analyses blew the gaff that adsorption occurs via physisorption, which was validated by the estimated ΔG^{0}_{ads} value in the limits of -27.311 kJ/mol to -23.889 kJ/mol, in adsorption studies. Furthermore, the linear correlation coefficient R^2, equal to 0.99, asserts adsorption obeying Langmuir isotherm. Overall, the oxazolones specified herein in this report can be recommended as probable corrosion inhibitors for API5L X60 steel used in transmission pipes of the oil and gas industries.

Funding

This research has no funding.

Acknowledgments

The authors acknowledge the Local management of OIL headed by Shri P Borkakaty (RCE), Shri S Datta Gupta (CGM- Chemical), Dr. Neeraj Mathur (CGM-R&D), and Shri P J Sharma, Ex-Executive Director (Oil & Gas Pipeline Services and Projects) for supporting in initiating the Industry-Academia Collaborative study for the betterment of the two organizations. Acknowledgments are also due to the support provided by the technical staff of various Laboratories of Chemical and R&D departments of OIL and Dibrugarh University. The authors also acknowledge the North East Institute of Science and Technology (NEIST), *Jorhat*, Assam, for SEM and SEM-EDX analysis.

Conflicts of Interest

The authors declare that they have no known competing financial interests or personal relationships that could have appeared to influence the work reported in this paper.

References

1. Roberge, P.R. Handbook of Corrosion Engineering. 2nd edition, McGraw-Hill, New York, **2012**.
2. Trabanelli, G. Inhibitor: An Old Remedy of New Challenge. *Corros.* **1991,** *47*, 410-419, https://doi.org/10.5006/1.3585271.
3. Schmitt, G. Fundamental Aspects of CO_2 Corrosion Advances in CO_2 Corrosion. NACE Corrosion 84 Conference, Houston, **1984**, p.10.
4. Waard, C. De.; Lotz, U. Prediction of CO_2 Corrosion of Carbon Steel. NACE Corrosion 93 Conference, Houston, **1993**, p.69.
5. Tenreiro, C.A.P. Corrosion and Asset Integrity Management for Upstream Installation in the Oil/Gas Industry. Publisher: Basenji Studios, LLC, **2016**, 1-370.
6. Aslam J.; Aslam, R.; Zehra, S.; Rizvi, M. Corrosion Inhibitors for Sweet (CO_2 corrosion) and Sour (H_2S Corrosion) Oilfield Environments. *Environmentally Sustainable Corrosion Inhibitors* **2022**, 165-181, https://doi.org/10.1016/B978-0-323-85405-4.00021-5.
7. Bentiss, F.; Traisnel, M.; Lagrenee, M. The Substituted 1,3,4-Oxadiazoles: A New Class Corrosion Inhibitor of Mild Steel in Acidic Media. *Corros. Sci*. **2000**, *42*, 127-146, https://doi.org/10.1016/S0010-938X(99)00049-9.

8. Bentiss, F.; Jama, C.; Mernari, B.; El Attari, H.; El Kadi, L.; Lebrini, M.; Lagrenee, M.; Traisnel, M. Corrosion Control of Mild Steel Using 3,5-Bis (4-Methoxyphenyl)-4-Amino-1,2,4-Triazole in Normal Hydrochloric Acid Medium. *Corros. Sci.* **2009**, *51*, 1628-1635, https://doi.org/10.1016/j.corsci.2009.04.009.
9. Haruna, K.; Saleh, T.A.; Quraishi, M.A. Expired Metformin Drug as Green Corrosion Inhibitor for Simulated Oil/Gas Well Acidizing Environment, *J. Mol. Liq.* **2020,** *315*, 113716, https://doi.org/10.1016/j.molliq.2020.113716.
10. Sigircik, G.; Tuken, T.; Erbil, M. Assessment of the Inhibition Efficiency of 3,4-diaminobenzonitrile Against the Corrosion of Steel. *Corros. Sci*. **2016,** *102*, 437-445, https://doi.org/10.1016/j.corsci.2015.10.036.
11. Rodriguez-Gomez, F.J.; Valdelamar, M.P.; Vazquez, A.E.; Perez, P.D.V.; Mata, R.; Miralrio, A.; Castro, M. Mycophelonic Acid as a Corrosion Inhibitor of Carbon Steel in 3 % wt. NaCl Solution: An Experimental and Theoretical Study. *J. Mol. Struct.* **2019,** *1183*, 168-181, https://doi.org/10.1016/j.molstruc.2018.12.035.
12. Obot, I.B.; Ul-Haq, M.I.; Sorour, A.A.; Alanazi, N.M.; Al-Abeedi, T.M.; Ali, S.A.; Al-Muallem, H.A. Modified Poly-aspartic Acid Derivatives as Effective Corrosion Inhibitor for C1018 Steel in 3.5% NaCl Saturated CO_2 Brine Solution. *J. Taiwan Inst. Chem. Eng.* **2022**, *135*, 104393, https://doi.org/10.1016/j.jtice.2022.104393.
13. Finsgar, M.; Petovar, B.; Xhanari, K.; Maver, U. Corrosion Inhibition of Certain Azoles on Steel in Chloride Media: Electrochemistry and Surface Analysis. *Corros. Sci.* **2016,** *111*, 370-381, https://doi.org/10.1016/j.corsci.2016.05.028.
14. Ontiveros-Rosales, M; Espinoza-Vezquez, A; Gomez, F.J.R.; Valdez-Rodriguez, S.; Miralrio, A.; Acosta-Garcia, B.A.; Castro, M. Imidazolate of 1-butyl-3-ethyl Imidazole as Corrosion Inhibitor on API 5L X52 Steel in NaCl Saturated with CO_2. *J. Mol. Liq.* **2022**, *363*, 119826, https://doi.org/10.1016/j.molliq.2022.119826.
15. Qian, S.; Cheng, Y.F. Synergistisism of Imidazoline and Sodium dodecylbenzenesulphonate Inhibitors on Corrosion Inhibition of X52 Carbon Steel in CO_2-Saturated Chloride Solutions. *J. Mol. Liq.* **2019**, *294*, 111674, https://doi.org/10.1016/j.molliq.2019.111674.
16. Wang, Y.; Yang, Z.; Hu, H.; Wu, J.; Finsagar, M. Indolizine Quaternary Ammonium Salt Inhibitors: The Inhibition and Anticorrosion Mechanism of New Dimer Derivatives from Ethyl Acetate Quinolinium Bromide and n-butyl Quinolinium Bromide. *Colloids Surf. A: Physicochem. And Eng. Asp.* **2022,** *651*, 129649, https://doi.org/10.1016/j.colsurfa.2022.129649.
17. Guo, Y.; Xue, J.; Zhang, J.; Chen, Q.; Fan, L.; Tang, C.; Ren, K.; Fu, A.; Bi, Q. Effect of Corrosion Products on the Inhibitory Performance of Imidazolium Ionic Liquid toward Carbon Steel in CO_2-Saturated NaCl Brine. *Colloids Surf. A: Physicochem. And Eng. Asp.* **2022**, *651*, 129135, https://doi.org/10.1016/j.colsurfa.2022.129135.
18. Abd El-Lateef, H.M.; Shalabi, K.; Tantawy, A.H. Corrosion Inhibition and Adsorption Features of Novel Bio-active Cationic Surfactants Bearing Benzinesulphonamide on C1018 Steel under Sweet Conditions: Combined Modeling and Experimental Approaches. *J. Mol. Liq.* **2020,** *320*, 114564, https://doi.org/10.1016/j.molliq.2020.114564.
19. Wang, X.; Wang, B.; Wang, Q.; Li, R.; Liu, H.; Jiang, H.; Liu, J. Inhibition Effect and Adsorption Behavior of Two Pyrimidine Derivatives as Corrosion Inhibitors for Q235 Steel in CO_2-Saturated Chloride Solution. *J. Electroanal. Chem.* **2021**, *903*, 115827, https://doi.org/10.1016/j.jelechem.2021.115827.
20. Shamsa, A.; Barmatov, E.; Hughes, T.L.; Hua, Y.; Neville, Y.; Barker, R. Hydrolysis of Imidazoline Based Corrosion Inhibitor and Effects on Inhibition Performance of X65 Steel in CO_2 Saturated Brine. *J. Petrol. Sci. Eng*. **2022**, *208*, 109325, https://doi.org/10.1016/j.petrol.2021.109235.
21. Zhang, Q.H.; Hou, B.S.; Li, Y.Y.; Lei, Y.; Wang, X.; Liu, H.F.; Zhang, G.A. Two Amino Acid Derivatives as High Efficient Green Inhibitors for the Corrosion of Carbon Steel in CO_2-Saturated Formation Water. *Corr. Sci*. **2021**, *189*, 109596, https://doi.org/10.1016/j.corsci.2021.109596.
22. Berdimurodov, E.; Kholikov, A.; Akbarov, K.; Guo, L. Inhibition Properties of 4,5-dihydroxy-4,5-di-ptolylimidazolidine-2-thione for Use on Carbon Steel in an Agressive Alkaline Medium with Chloride Ions: Thermodynamic, Electrochemical, Surface and Theoretical Analyses. *J.Mol. Liq.* **2021**, *327*, 114813, https://doi.org/10.1016/j.molliq.2020.114813.
23. Saady, A.; Rais, Z.; Benhiba, F.; Salim, R.; Alaoui, K.I.; Arrousse, N.; Elhajjaji, F.; Taleb, M.; Jarmoni, K.; Rodi, Y.K.; Warad, I.; Zarrouk, A. Chemical, Electrochemical, Quantum, and Surface Analysis Evaluation on the Inhibition Performance of Novel Imidazo[4,5-b] pyridine Derivatives Against Mild Steel Corrosion. *Corr. Sci*. **2021**, *189*, 109621, https://doi.org/10.1016/j.corsci.2021.109621.

24. Burahgohain, P.; Sharma, G. A Descriptive Study on the Use of Nanomaterials as Corrosion Inhibitors in Oil and Gas Industry. *Int J Sci Techno Res.* **2019**, *8*, 3999-4002.
25. Sharma, N.; Banerjee, J.; Shrestha, N.; Chaudhury, D. A Review on Oxazolone, Its Method of Synthesis and Biological Activity. *European J. Biomed. Pharm. Sci*. **2015**, *2*, 964-987.
26. Muthoboopathi, G. Synthesis Characterization and Biological Evaluation of Oxazolone Analogs. *Asian J. Pharm. Clinical Res.* **2018,** *11*, 159-162, https://doi.org/10.22159/ajpcr.2018.v11s4.31726.
27. Sharma, G.; Burhagohain, P. Evaluation of Percentage Corrosion Inhibition Efficiency of Mild Steel with Derivatives of Oxazolone. *J. Adv. Appl. Sci. Res.* **2021**, *3*, 16-24, http://joaasr.com/index.php/joaasr/article/view/114.
28. Burhagohain, P.; Sharma, G.; Bujarbaruah, P.M. Investigation of a few Oxazolone Molecules as Corrosion Inhibitor for API5LX60 Steel in 1N H_2SO_4 Solution. *Egyptian J. Petrol.* **2022**, *31*, 37-45, http://doi.org/10.1016/j.ejpe.2022.06.006.
29. Sharma, G.; Handique, J.G. Synthesis of a Series of Low Band Gap Small Organic Molecules and the Evaluation of their Solar Cell Acivity. *Asian J. Chem.* **2016**, *28*, 2223-2227, http://dx.doi.org/10.14233/ajchem.2016.19931.
30. Vogel, A.I.; Tatchell, A.R.; Furniss, B.S.; Hannaford, A.J.; Smith, P.W.G. Vogel's Textbook of Practical Organic Chemistry. 5th ed., Prentice Hall, **1989**.
31. Kousar, K.; Walczak, M.S.; Ljungdahi, T.; Wetzel, A.; Oskarsson, H.; Restuccia, P.; Ahmad, E.A.; Harrison, N.M.; Lindsay, R. Corrosion Inhibition of Carbon Steel in Hydrochloric Acid: Elucidating the Performance of an Imidazoline-Based Surfactant. *Corr. Sci*. **2021**, *180*, 109195, https://doi.org/10.1016/j.corsci.2020.109195.
32. ASTM-G3. Standard Practice Conventions Applicable to Electrochemical Measurements in Corrosion Testing. **2019.**
33. Nooshabadi, M.; Ghandchi, M.S. *Santolina chamaecyparissus* Extract as Natural Source Inhibitor for 304 Stainless Steel Corrosion in 3.5% NaCl. *J. Ind. Eng. Chem.* **2015**, *31*, 231-237, http://dx.doi.org/doi:10.1016/j.jiec.2015.06.028.
34. Li, X.; Deng, S.; Fu, H. Triazolyl Blue Tetrazolium Bromide as a Novel Corrosion Inhibitor for Steel in HCl and H_2SO_4 Solutions. *Corros. Sci.* **2011,** *53*, 302–309, https://doi.org/10.1016/j.corsci.2010.09.036.
35. Abdallah, M.; Al-Gorair, A.S.; Fawzy, A.; Hawsawi, H.; Hameed, R.S.A. Enhancement of Adsorption and Anticorrosion Performance of Two Polymeric Compounds for the Corrosion of SABIC Carbon Steel in Hydrochloric Acid. *J. Adhes. Sci. Technol.* **2022,** *36*, 35-53, https://doi.org/10.1080/01694243.2021.1907041.
36. Larif, M.; Elmidaoui, A.; Zarrouk, A.; Zarrouk, H.; Salghi, R.; Hammouti, B.; Oudda, H.; Bentiss, F. An Investigation of Carbon Steel Corrosion Inhibition in Hydrochloric Acid Medium by an Environmentally Friendly Green Inhibitor. *Res. Chem. Intermed.* **2013,** *39*, 2663–2677, https://doi.org/10.1007/s11164-012-0788-2.
37. Xiong, L.; Wang, P.; He, Z.; Chen, Q.; Pu, J.; Zhang, R. Corrosion Behaviors of Q235 Carbon Steel Under Imidazoline Derivatives as Corrosion Inhibitors: Experimental and Computational Investigations. *Arabian J. Chem.* **2021**, *14*, 102952, https://doi.org/10.1016/j.arabjc.2020.102952.
38. Bouoidina, A.; Ech-chihbi, E.; El-Hajjaji, F; El Ibrahibi, B.; Kaya, S.; Taleb, M. Anisole Derivatives as Sustainable-Green Inhibitors for Mild Steel Corrosion in 1 M HCl: DFT and Molecular Dynamic Simulations Approach. *J. Mol. Liq.* **2021**, *324*, 115088, https://doi.org/10.1016/j.molliq.2020.115088.